pISSN 2384-1095
eISSN 2384-1109

iMRI 2020;24:196-206

https://doi.org/10.13104/imri.2020.24.4.196

iMRI
Investigative Magnetic Resonance Imaging

Deep Learning in MR Motion Correction: a Brief Review and a New Motion Simulation Tool (view2Dmotion)

Seul Lee, Soozy Jung, Kyu-Jin Jung, Dong-Hyun Kim

Department of Electrical and Electronic Engineering, Yonsei University, Seoul, Korea

With the development of deep-learning techniques, the application of deep learning in MR imaging processing seems to be growing. Accordingly, deep learning has also been introduced in motion correction and seemed to work as well as do conventional motion-compensation methods. In this article, we review the motion-correction methods based on deep learning, focusing especially on the motion-simulation methods adopted. We then propose a new motion-simulation tool, which we call view2Dmotion.

Keywords: Deep learning; Machine learning; Motion artifact; Motion correction; Motion simulation

Review Article

Received: October 15, 2020
Revised: October 15, 2020
Accepted: November 11, 2020

Correspondence to:
Dong-Hyun Kim, Ph.D.
Department of Electrical and Electronic Engineering, Yonsei University, 50-1 Yonsei-ro, Seodaemun-gu, Seoul 03722, Korea.
Tel. +82-2-2123-5874
Fax. +82-2-313-2879
E-mail: donghyunkim@yonsei.ac.kr

INTRODUCTION

Magnetic resonance imaging (MRI) is a non-invasive soft-tissue mapping technique, which is widely used to diagnose various diseases without radiation exposure. However, MRI is sensitive to movement of the subject because of the long acquisition time, which causes motion artifacts (1). The subject's motion creates incorrect allocation values of the *k*-space signal from MRI machines and results in blurring or ghosting artifacts (1, 2), which can be typically observed in the reconstructed images. Additionally, technological developments in MR hardware have improved spatial resolution and signal-to-noise ratio (SNR), but can be more susceptible to motion artifacts because of extended scan times (1, 3, 4). Most importantly, in clinical settings, these motion artifacts may affect the diagnosis for patients who cannot control their movements. Thus, the subject motion is an important factor that has been continuously considered in MR imaging.

To address motion-related problems, there have been many methods to prevent motion or to correct artifacts. The basic straightforward method is to make restrain patients' motions by means of sedation or breath-holding (5, 6). However, since this method asks the patient to actively control motions, there was also an effort to use the parallel imaging technique in order to reduce the burden on the patient (7, 8). This method can reduce scan times with fewer phase encodings during MR scanning, but it is still affected by artifacts from patients who cannot control their behavior. In terms of MR systems, MR navigators (9-13), which are additional pulses to track motion or motion-tracking systems, such as an in-bore camera and markers (14-18), are generally used to measure the patient's motion. Using trajectory information, these prospective methods compensate for or reacquire the *k*-space partially during data acquisition (3,

12, 15-23), although retrospective methods, which process the data after the MR acquisition (4, 24-27), could also be considered for the motion correction. In addition, these retrospective methods could be executed with algorithms estimating motion without acquiring motion information. However, the computational limits are evident because of the complex and unpredictable patient motions in this case (28, 29). Overall, these conventional methods incur additional cost, such as from prolonged scan time (30, 31) and modification of sequences.

Recently, deep learning has shown remarkable acceptability in MR image processing (28). Also, it has been suggested to use deep learning for the motion correction as an alternative method, since it does not require any additional scan time, motion-tracking systems, or alteration of sequence. In this process, a neural network is trained with an enormous training dataset, which typically consists of motion-corrupted images as an input and motion-clean images as a label. To generate motion-corrupted images, motion simulations in the image domain (29-32) or *k*-space domain (33-36) are essential. However, since these previous studies considered only simple and fixed motion patterns, applications to various motion artifacts from patients whose motions are unexpected to have limitations (31). Thus, network training requires new data-generation methods to consider the motion artifacts generated for various reasons.

In this paper, we review previous studies for motion-correction methods based on deep learning. In particular, we pay attention to the methods used for network training. We then propose a new motion-simulation tool, called view2Dmotion, which can generate massive training datasets for motion simulation.

Description of Motion

MR data acquisition proceeds in its Fourier domain, i.e., *k*-space. Each data point in *k*-space corresponds to the frequency content of the image, and the alteration of a single point in *k*-space influences the whole image. When motion occurs during MR acquisition, errors occur in *k*-space that can cause blurring and/or ghosting in the image domain. Generally in 2DFT scans, motion artifacts are observed in the phase-encoding direction, since the time to acquire a single sample in the frequency-encoded direction is on the order of milliseconds, which is much faster than is the subject's movement (5). Subject motion frequently observed in MR images can be classified into two main types: non-rigid motion and rigid motion (1, 37).

Non-rigid motion or elastic motion is the involuntary deformation movement that is caused by physiological factors (38). In detail, this can be categorized into periodic and/or continuous motion, such as respiration, CSF flow, and peristalsis, and sudden involuntary motion, such as swallowing and coaching (1, 37). The periodic motion produces ghosting artifacts, where the random motion shows blurring in the reconstructed image (5, 39). These types of motion artifacts are usually observed in the abdomen, where various deformation movements occur (1).

Rigid motion is caused by the subject's unspontaneous or voluntary random movement (39). This type of movement can be observed in all parts of the body, especially in the brain. Also, it occurs more frequently in the non-compliant subjects, such as children or subjects affected by degenerative diseases of the nervous system, such as Parkinson's (37). Rigid motion is generally represented by six parameters, indicating three translations and three rotations (1).

Motion parameters can be inferred directly from the raw data by minimizing the motion-related image-quality metric or data-consistency error. However, these approaches are still challenging because of the non-convex nature of estimation and long processing time, limiting the integration into clinical MRI scans (28, 31).

Motion Correction Based on Deep Learning

Deep learning has been introduced for reducing motion artifacts without the need for supplementary data acquisition (6, 31, 40, 41). Generally, the motion correction proceeds in the image domain, where training is done with a motion-corrupted image as an input and motion-clean image as a label. In particular, since the shape of the motion artifact depends on the type of motion, as shown in Figure 1, most studies set their scope to a specific motion type. The summary for the following comprehensive review information is shown in Table 1 for non-rigid motion and in Table 2 for rigid motion.

Non-Rigid Motion

Despite the implementation of instructions or sedation to prevent motion, non-rigid respiratory motion occasionally occurs because of the discomfort of the subject during the scan (5).

U-net architecture, which has worked well in various

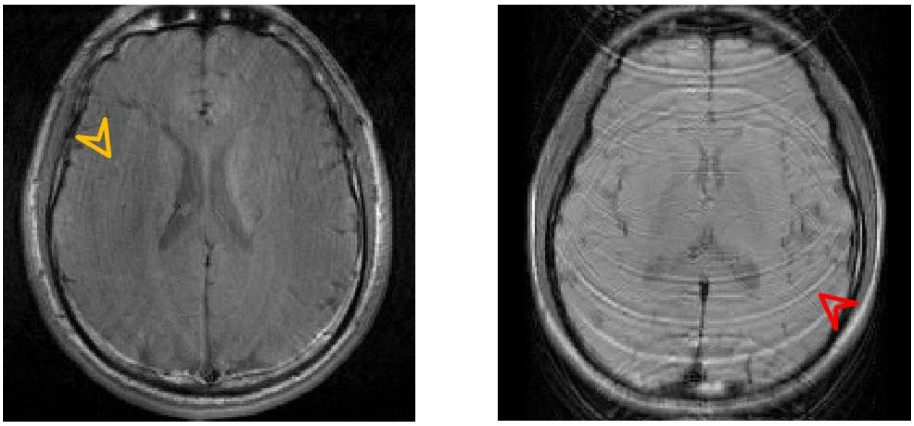

Fig. 1. Motion artifacts. (a) blurring, and (b) ghosting.

Table 1. **Summary of Deep-Learning-Based Non-Rigid Motion-Correction Methods**

Purpose	Model	Motion simulation	Author	Dataset			Commentary	Reference number
				Input	Label	Test		
Respiratory motion artifact compensation	U-net	X	Lee et al.	Real motioncorrupted image	ID-Navigator compensated image	Real motioncorrupted image	Data augmentation (horizontal flip)	43
	CNN based MARC	Periodic and random respiratory motion in kspace domain	Tamada et al.	Simulated motioncorrupted image	Artifact component image	Simulated motioncorrupted image	Patch-wise learning	35
	Improved MARC		Kromrey et al.	Simulated motioncorrupted image	Artifact component image	Simulated motioncorrupted image	X	44

medical imaging tasks, has also been used for motion correction (42). Lee et al. (43) used the U-net to reduce the ghosting artifacts caused by respiratory motion. Here, the real data compensated for by 1D-Navigator was used as a label, then data augmentation was applied to overcome the lack of data by flipping horizontally. The artifact caused by the respiratory motion was reduced in this study, although it showed slight blurring.

Other convolutional neural networks (CNN) have also been applied for the correction. Tamada et al. (35) proposed a multi-channel CNN-based model: motion artifact reduction using a convolutional neural network (MARC), with a patch-wise image to increase the training data and to use memory efficiently. It was trained to optimize the residual between the simulated artifact and ground-truth images and that between the simulated artifact and predicted images. With improved performance using MARC, they applied the MARC filter in gadoxetate disodium-enhanced arterial-phase liver MRI and demonstrated substantial artifact reduction (44).

Rigid Motion

Rigid motion is more prevalent in the brain, which is less affected by respiration and peristalsis, than in the other body regions, such as abdomen and chest (37).

Johnson and Drangova (45) provided one of the first studies for motion-correction reconstruction using deep learning. The motion-corrected magnitude MR image was reconstructed from the vector of motion-deformed *k*-space by the deep neural network (DNN). This study showed the potential of deep-learning-based motion-correction methods.

Pawar et al. (30, 31) suggested the standard U-net model for motion correction (MoCoNet), which generates the motion-compensated image from the motion-corrupted image with a 3D magnetization prepared rapid acquisition gradient echo (MPRAGE) image. However, it was trained by simulated data, and the simulation patterns were restricted to simple sudden motion. This group further proposed a more realistic motion-simulation method with improved

Table 2. Summary of Deep-Learning-Based Rigid Motion-Correction Methods

Purpose	Model	Motion simulation	Author	Dataset			commentary	Reference number
				Input	Label	Test		
Motion artifact Compensation	DNN	Phase shift and rotation in kspace domain	Johnson et al.	Vector of motion deformed k-space data	Motion-corrected image	Vector of motion deformed k-space data	X	45
	FCN	Sudden and oscillating motion in k-space domain	Sommer et al.	Simulated motioncorrupted image	Artifact-filtered image	Simulated motioncorrupted image	Using multi-resolution images	33
	MoCoNet (encoder-decoder U-net)	Random motion in image domain	Pawar et al.	Simulated motioncorrupted image	Motion-corrected image	Real motion-corrupted 3D MPRAGE data	X	30,31
	Improved MoCoNet		Pawar et al.	Simulated motioncorrupted image	Motion-corrected image	Real motion-corrupted data	Using Inception-ResNet for encoder network	32
	Deep CNN		Dou et al.	Simulated motioncorrupted image	Motion-corrected image	Simulated motioncorrupted image	Using spiral and cartesian trajectories as input	49
		Random motion in k-space domain	Bydder et al.	Simulated motioncorrupted 8 coil sets of the k-space data	Phase encode index	Simulated motioncorrupted 8 coil sets of the k-space data	Using deep learning for motion detection	50
			Haskell et al.	Simulated motioncorrupted image	Artifact-only image	Simulated motioncorrupted image	Patch-wise learning, Machine learning with model-based method	36
			Duffy et al.	Simulated motioncorrupted image	Motion-free image	Real motion-corrupted data	X	34, 46
	GAN	Translation and rotational motion in image domain	Usman et al.	Simulated motioncorrupted image	Motion-corrected image	Simulated motioncorrupted image	Using various trajectory methods	48
PET-CT translation, MR motion correction, PET denoising	MedGAN (GAN-guided Unet)	X	Armanious et al.	PET image/ Motioncorrupted MR image/ Noisy PET image	CT image / Motionfree MR image/ Denoised PET image	PET image/ Motioncorrupted MR image/ Noisy PET image	Using New generator model (CasNet)	40, 47
Out-of-FOV motion artifacts correction	Modified U-net	Sudden and oscillating motion in image domain	Wang et al.	Simulated motioncorrupted image	Motion-free image	Simulated motioncorrupted image	X	29

MoCoNet (32). This method implemented linear combination of rigidly transformed data and clear images. The Inception-ResNet network was trained with this motion-simulated image and exceeded the entropy-minimization method.

Sommer et al. (33) applied data augmentation to increase the data fluctuation before the motion artifact simulation. Then, fully convolutional neural networks (FCN) extracted motion artifact-only image, which subtracts the motion-clean image from the motion-corrupted image. Moreover, since multi-resolution images were adopted for training, there is less deformation in anatomical structures by the network-based filtering.

Duffy et al. (34, 46) used simulated data to train the regression CNN model that could predict motion-free images. The coherent simulated ghosting and severe motion were compensated for better than random artifacts and mild motion but smoothing occurred. The result from this study suggested that the neural network trained with the simulated data can eliminate the real motion artifact.

Armanious et al. (40, 47) proposed a new GAN framework, MedGAN, which contains the new generator model. Three U-net architectures were connected to improve the details of images by means of the encoder-decoder process, which reduces the blurriness and increases the capacity of the network. The validation was performed with three different tasks and showed noticeable achievement, not only in the MR motion correction but also in PET-CT translation and PET denoising. Additionally, the network was improved to the MedGAN joint, which is flexible for the rigid and non-rigid motion (6). When the data were obtained from various body regions, including the head and pelvis for rigid motion, and the abdomen for non-rigid motion, the result from this study improved the artifact reduction in both types of motion, though the diagnostic information could be lost.

The above-mentioned techniques were based on Cartesian sampling, whereas other trajectory showed different aspects of the artifact. Usman et al. (48) and Dou et al. (49) implemented various *k*-space trajectories, such as radial and spiral, to illustrate the motion artifact. Usman et al. (48) applied the GAN-based framework in the Cartesian sequential, Cartesian parallel, and random trajectories. Since the random trajectory was less influenced by motion than was the Cartesian, it showed the best achievement in the validation. Dou et al. (49) also used spiral and Cartesian trajectories as inputs of the deep CNN model separately to compare the results concerning the trajectory.

The conventional retrospective methods commonly correct the restricted artifacts in plane. For example, Wang et al. (29) proposed methods for correcting the out-of-FOV motion artifacts using modified U-net and motion parameters. The latter were applied to the loss function to reduce the complexity of computation, improve performance, and provide more robust motion-artifact correction than does the conventional gradient-based autofocusing algorithm.

Deep learning has been used not only for motion correction but also for detection. Bydder et al. (50) used the CNN model to detect the outliers in motion-corrupted *k*-space and eliminate the deformed *k*-space lines. A low-rank-based method was subsequently applied for the reconstruction. This study showed that it was possible to detect *k*-space deformation with deep learning.

Notably, Haskell et al. (36) proposed a motion-correction method called NAMER, which combined CNN and a model-based method. First, they trained the CNN to detect the motion artifacts, then used the motion-corrupted images and their corresponding motion-only artifacts as input and output of CNN; the difference between them was considered to be the initial motion-compensated image. Then, the motion parameters were estimated from the initial motion-compensated image and motion-corrupted image. Finally, the motion-mitigated image was generated by the model-based reconstruction using the calculated motion parameters. These three steps were repeated until they produced the optimized parameters and image. Combining the CNN and model-based reconstruction method, it was able to reduce the computing time, and have efficiency for the non-linear problem as well as high robust confidence in the final reconstruction. The result of their work outperformed only the CNN-based method to remove the motion artifact.

Motion Simulation

The above-mentioned deep-learning-based motion-correction techniques constructed training datasets with simulated motion. When acquiring real motion-corrupted and motion-clean datasets for training, this enforces long scan times and thus increases the cost of collecting the training data (40). Therefore, motion-simulation techniques have been inevitable for deep-learning-based motion correction. In this section, we summarize previous motion-simulation approaches used for motion-correction techniques. We limit the scope to rigid motion, which most of the simulation-based studies deal with. The current motion-simulation techniques can be broadly classified

into two categories: image-based approaches and *k*-space-based approaches.

Figure 2a shows the image-based motion-simulation approach. When raw *k*-space data are Fourier transformed into an MR image, motion parameters are applied to the motion-clean MR image. This process is repeated for n times, where n denotes the number of motion-corrupted *k*-space lines. The parameter range for the motion and the methods to choose the *k*-space lines have differed between the studies. Pawar et al. (31, 32) did motion simulation between ± 5 mm of translation and ± 5° of rotation. Wang et al. (29) proposed the range between 0.07 and 7 mm of translation and 0 to 20° of rotation. In choosing the motion-corrupted *k*-space lines, Pawar et al. (31, 32) used random selection, although several motion scenarios using full *k*-space lines have been suggested. For example, in Wang et al. (29), sudden motion, where the subject abruptly moves during the scan, and oscillating motion, where the subject continuously moves during the scan, are simulated. These motion scenarios demonstrated that motion-simulation techniques could cover a wide range of realistic motions.

Figure 2b shows the *k*-space-based motion-simulation approach. Raw *k*-space data are directly used for the

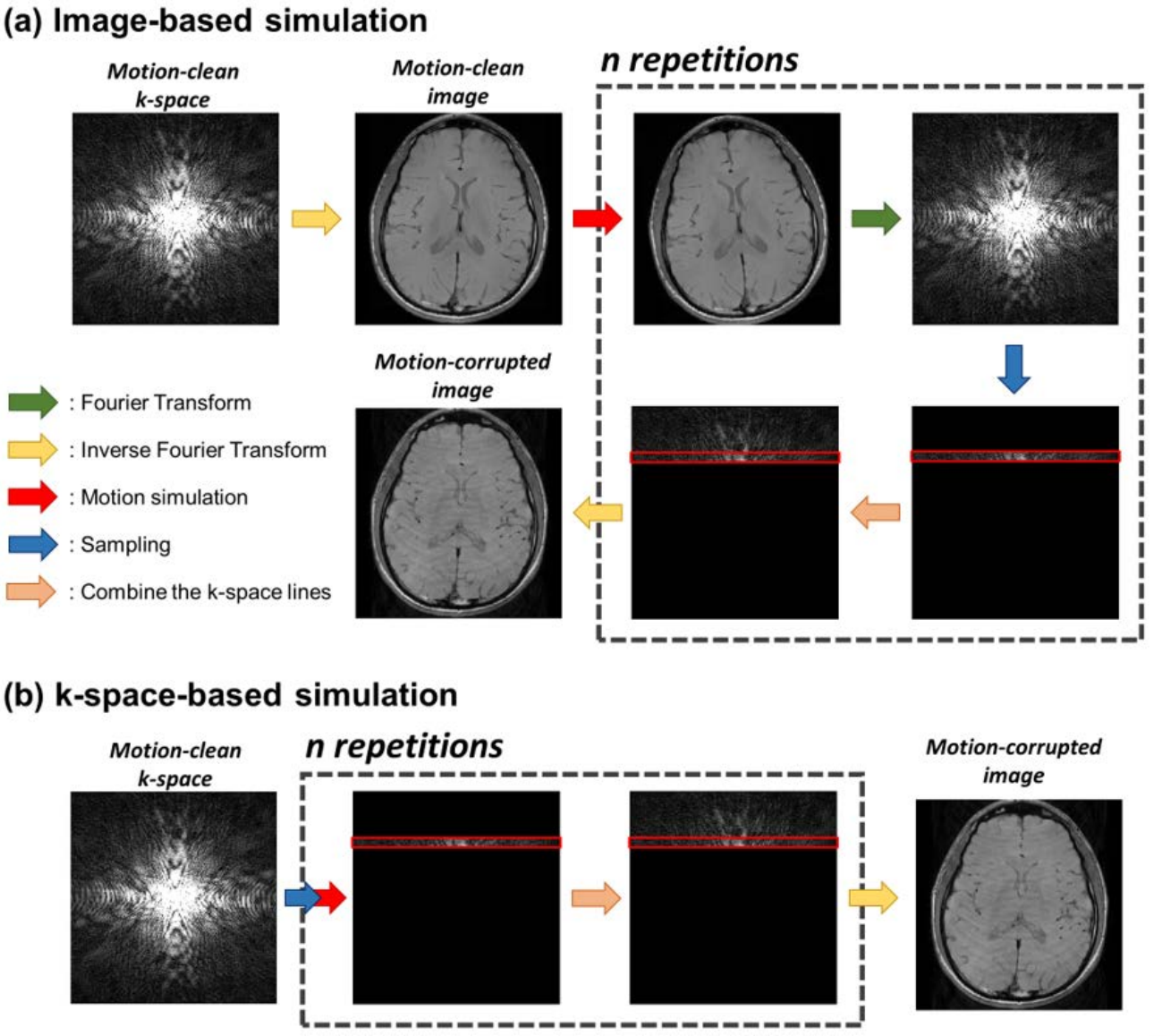

Fig. 2. The motion-simulation methods mentioned in Section 3. (a) image-based simulation, and (b) *k*-space-based simulation.

motion simulation using the shift and rotation theorems in Fourier transform. As in the image-based approaches, translation and rotation were implemented for the simulations. Sommer et al. (33) suggested translation with a range of 0.9 to 5.4 mm and rotation with a range of 1.0 to 2.5°. Several studies generated only translation motion. For motion-corrupted *k*-space line selection, Duffy et al. (34) used random selection, whereas several motion scenarios were used in Sommer et al. (33), Tamada et al. (35), and Kromrey et al. (44).

Additionally, some MR simulators offer motion-simulation functions internally (51, 52). These tools provide motion-simulated MR images using specific phantom data. However, since these simulators are not specific for motion, they can simulate only a simple movement pattern, which is insufficient for generating the massive training dataset needed for deep learning.

View2Dmotion: New Motion-Simulation Tool

The previous section indicates the significance of motion simulation in deep learning-based motion-correction techniques. Hence, we propose a new numerical motion-simulation package, View2Dmotion, with various motion-type options that could be used to generate the training dataset. This simulation was based on environment developing by MATLAB R2019b (The MathWorks, Natick, MA, USA).

Figure 3 shows the interface of the simulator, which is divided into four sections. Figure 3a is the display part that shows the original motion-clean image and the resultant motion-corrupted image. The motion-related option be selection is in Figure 3b, where several motion scenarios and the data to be simulated are selected. To simulate realistic motion, in this simulator, several sequence parameters used to acquire the data are needed, such as the sampling trajectory, phase-encoding direction, repetition time (TR), and total scan time. Options of the

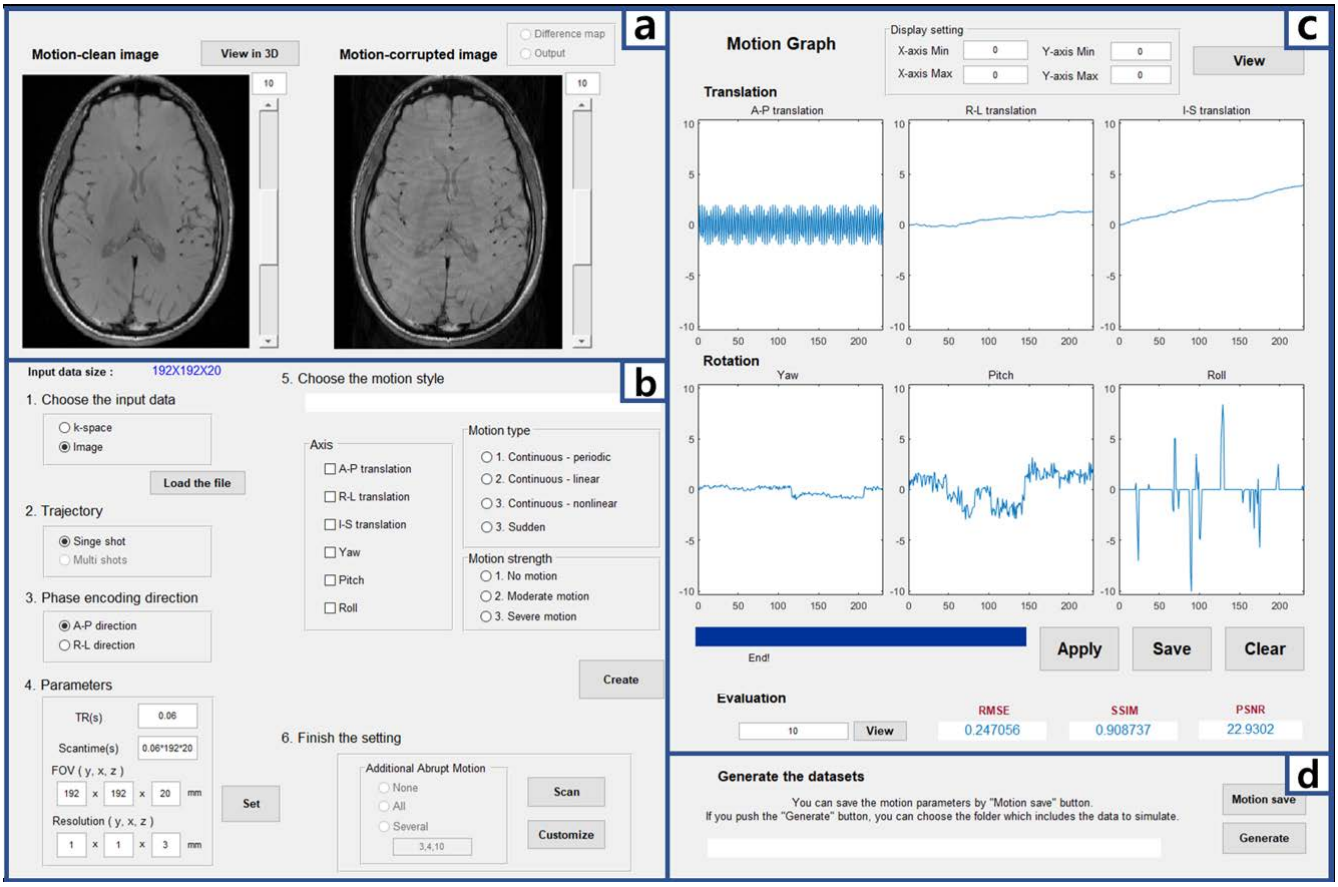

Fig. 3. Interface of view2Dmotion. (a) image display part, (b) motion scenario part, (c) motion parameter part, and (d) save and generate part.

movement can be selected as follows: axes of motion (A-P, R-L, and I-S translations and Yaw, Pitch, and Roll rotations), type of motion (continuous-periodic, continuous-linear, continuous-nonlinear, sudden), and strength of motion (no, moderate, severe). In detail, we can choose the axes of the motion. When we select the A-P, R-L, and I-S axes, the *k*-space-based motion-simulation is done as translation motion, and others are done as image-based rotation motion. The type of motion is divided into constant motion and sudden motion, which is generally handled in motion simulation. Furthermore, the strength of motion controls the amplitude of motion, and the 'no' option eliminates the motion of the pertinent axis.

Figure 4 shows the results from selecting a type of motion that can be simulated in this simulation tool. Figure 4a is generated from the continuous-periodic motion type within 0.2-0.7 Hz frequency, which generally correspond to respiratory motion (35, 53). The continuous-linear motion, continuous-nonlinear motion, and sudden motion are shown in Figure 4b-d, which represent the subject's rigid motion. The subject's motion that is shifted in one side consistently could be formed by the continuous-linear motion type. Also, the continuous-nonlinear motion which depicts tossing and turning is generated by adding nonlinearity to linear motion. In particular, sudden motions are generated by setting the number and range of peaks randomly in Figure 4d; these can represent sneezing, swallowing, and yaw. Figure 4 is just an example, and this simulator provides a vast number of motion scenarios in this way. Thus, it is possible to generate innumerable motion-corrupted images from only one dataset.

When the selection of motion scenario is finished, these actual motion dimensions are shown graphically in Figure 3c. Now, motion can be applied to the motion-clean

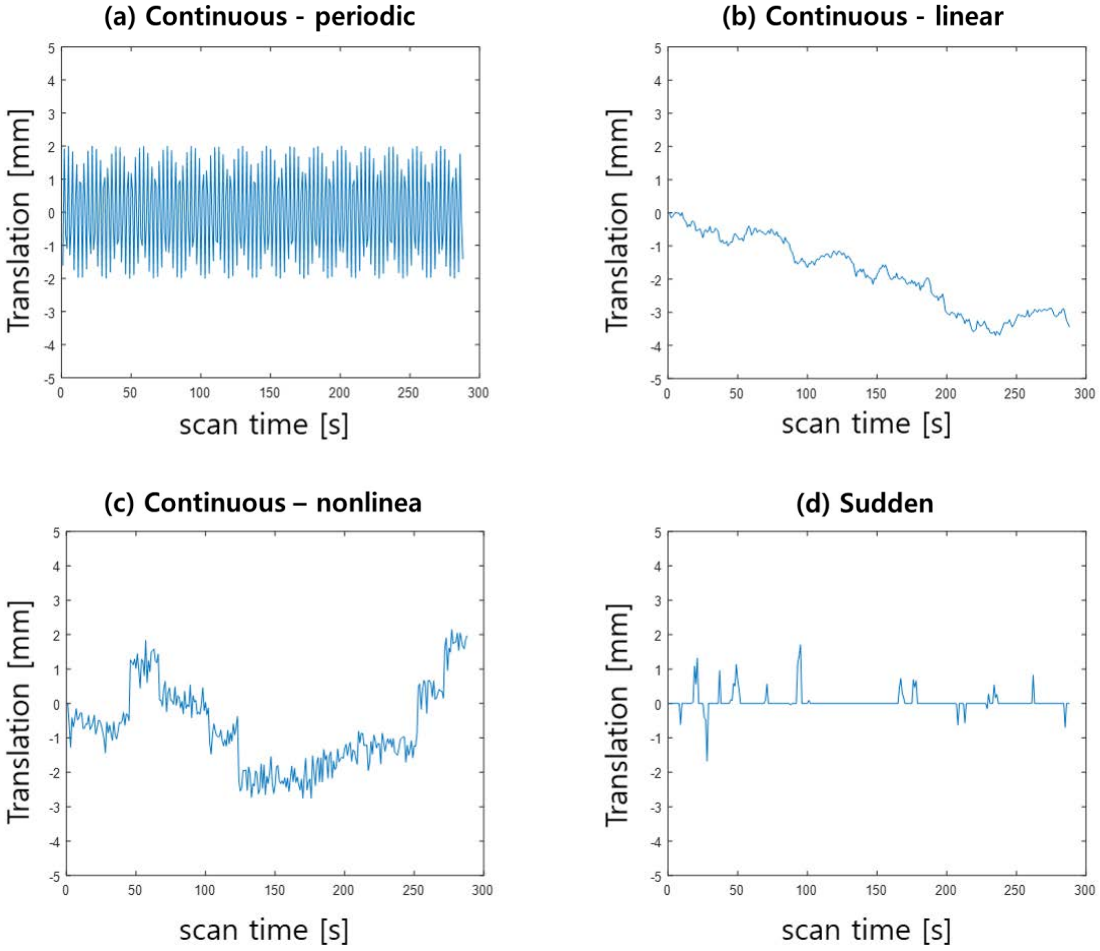

Fig. 4. Images (a-d) are a motion parameters graph, which is generated by view2Dmotion. (a) Periodic motion, (b) linear motion, (c) nonlinear motion, (d) sudden motion.

image, and the motion parameters along with the motion-corrupted image are saved. To analyze the simulated motion quantitatively, root mean square error (RMSE), structural similarity index (SSIM), and peak signal-to-noise ratio (PSNR) are also displayed. These indexes can be described as follows:

$$RMSE = \sqrt{\frac{\sum_{x=1}^{Nx}\sum_{y=1}^{Ny}(r(x,y) - m(x,y))^2}{N_x N_y}}$$

$$SSIM = \frac{(2\mu_r \mu_m + C_1)(2\sigma_{rm} + C_2)}{(\mu_r^2 + \mu_m^2 + C_1)(\sigma_r^2 + \sigma_m^2 + C_2)}$$

$$PSNR = 10\log_{10}\left[\frac{\sum_{x=1}^{Nx}\sum_{y=1}^{Ny} r(x,y)^2}{\sum_{x=1}^{Nx}\sum_{y=1}^{Ny}(r(x,y)-m(x,y))^2}\right]$$

where N_x, N_y are the total number of pixels in the 2D image, r and m represent the reference motion-clean image and motion-corrupted image, μ_r, μ_m, σ_r, σ_m, and σ_{rm} are local mean, standard deviation, and cross-covariance of motion-clean and motion-corrupted images, and C_1 C_2 are constant values embedded in MATLAB. These indexes are calculated with normalized motion-corrupted and motion-clean images by min-max normalization. Since the purpose of this simulator is to generate the training dataset for deep learning, in Figure 3d, we can upload bulk datasets and generate the motion-corrupted dataset. Since it works for 2D images, however, it could extend to the application to 3D images and consider other scan options, such as multi slicing, in a further study.

Figure 5 shows examples of motion-corrupted images using this simulator. These spin-echo (SE) data were simulated identically with the following parameters: single shot, TR = 60 ms, image resolution = 1 × 1 × 3 mm^3, strength of motion = moderate. The resultant images in the first row are simulated with translation motion along the A-P phase-encoding direction, and the second-row images are simulated with rotation motion along R-L phase-encoding direction. Therefore, the motion artifacts are observed in the A-P direction in the first-row images and the R-L direction in the second-row images.

CONCLUSION

In conclusion, studies on compensating for patients' motions have been proposed continuously. This article introduced motion-correction research using deep learning. The deep-learning-based motion-correction method require neither supplementary motion-tracking hardware systems, modification of acquisition sequence, nor image-reconstruction methods.

Additionally, we suggest a new motion-simulation tool, view2Dmotion. It not only adapts translations and rotations, but also can generate new motion parameters. Therefore, it can facilitate generating a vast amount of realistic datasets for motion correction needed for deep learning.

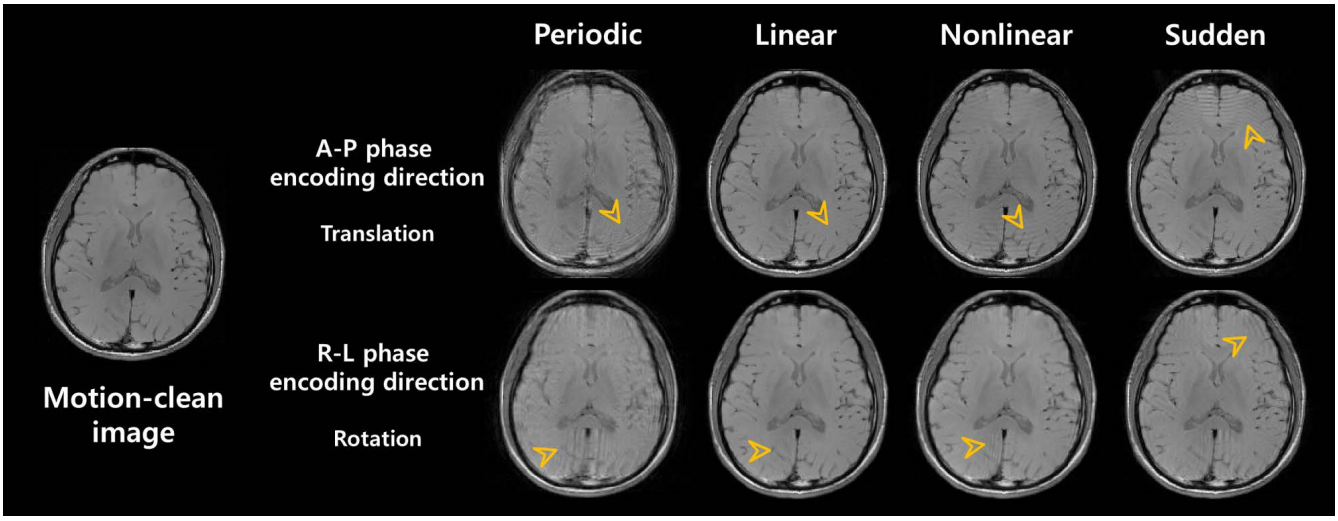

Fig. 5. Motion-corrupted images generated by view2Dmotion. Simulation could be done along two encoding directions, A-P and R-L, for motion types: Continuous motion (periodic, linear, nonlinear) and sudden motion.

Acknowledgments

This work was supported by the National Research Foundation of Korea (NRF) grant funded by the Korean government (MSIT) (NRF-2019R1A2C1090635) and by the advanced MR study group of KSMRM (2020).

REFERENCES

1. Zaitsev M, Maclaren J, Herbst M. Motion artifacts in MRI: a complex problem with many partial solutions. J Magn Reson Imaging 2015;42:887-901
2. Heiland S. From A as in aliasing to Z as in zipper: artifacts in MRI. Clin Neuroradiol 2008;18:25-36
3. Stucht D, Danishad KA, Schulze P, Godenschweger F, Zaitsev M, Speck O. Highest resolution in vivo human brain MRI using prospective motion correction. PLoS One 2015;10:e0133921
4. Gallichan D, Marques JP, Gruetter R. Retrospective correction of involuntary microscopic head movement using highly accelerated fat image navigators (3D FatNavs) at 7T. Magn Reson Med 2016;75:1030-1039
5. Stadler A, Schima W, Ba-Ssalamah A, Kettenbach J, Eisenhuber E. Artifacts in body MR imaging: their appearance and how to eliminate them. Eur Radiol 2007;17:1242-1255
6. Armanious K, Gatidis S, Nikolaou K, Yang B, Kustner T. Retrospective correction of rigid and non-rigid MR motion artifacts using GANs. IEEE 16th International Symposium on Biomedical Imaging (ISBI), 2019
7. Noel P, Bammer R, Reinhold C, Haider MA. Parallel imaging artifacts in body magnetic resonance imaging. Can Assoc Radiol J 2009;60:91-98
8. Hamilton J, Franson D, Seiberlich N. Recent advances in parallel imaging for MRI. Prog Nucl Magn Reson Spectrosc 2017;101:71-95
9. Fu ZW, Wang Y, Grimm RC, et al. Orbital navigator echoes for motion measurements in magnetic resonance imaging. Magn Reson Med 1995;34:746-753
10. McGee KP, Felmlee JP, Manduca A, Riederer SJ, Ehman RL. Rapid autocorrection using prescan navigator echoes. Magn Reson Med 2000;43:583-588
11. Johnson PM, Taylor R, Whelan T, Thiessen JD, Anazodo U, Drangova M. Rigid-body motion correction in hybrid PET/MRI using spherical navigator echoes. Phys Med Biol 2019;64:08NT03
12. Tisdall MD, Hess AT, Reuter M, Meintjes EM, Fischl B, van der Kouwe AJ. Volumetric navigators for prospective motion correction and selective reacquisition in neuroanatomical MRI. Magn Reson Med 2012;68:389-399
13. Mendes J, Kholmovski E, Parker DL. Rigid-body motion correction with self-navigation MRI. Magn Reson Med 2009;61:739-747
14. Schulz J, Siegert T, Reimer E, et al. An embedded optical tracking system for motion-corrected magnetic resonance imaging at 7T. MAGMA 2012;25:443-453
15. Zaitsev M, Dold C, Sakas G, Hennig J, Speck O. Magnetic resonance imaging of freely moving objects: prospective real-time motion correction using an external optical motion tracking system. Neuroimage 2006;31:1038-1050
16. Qin L, van Gelderen P, Derbyshire JA, et al. Prospective head-movement correction for high-resolution MRI using an in-bore optical tracking system. Magn Reson Med 2009;62:924-934
17. Todd N, Josephs O, Callaghan MF, Lutti A, Weiskopf N. Prospective motion correction of 3D echo-planar imaging data for functional MRI using optical tracking. Neuroimage 2015;113:1-12
18. Ooi MB, Krueger S, Thomas WJ, Swaminathan SV, Brown TR. Prospective real-time correction for arbitrary head motion using active markers. Magn Reson Med 2009;62:943-954
19. Maclaren J, Herbst M, Speck O, Zaitsev M. Prospective motion correction in brain imaging: a review. Magn Reson Med 2013;69:621-636
20. Callaghan MF, Josephs O, Herbst M, Zaitsev M, Todd N, Weiskopf N. An evaluation of prospective motion correction (PMC) for high resolution quantitative MRI. Front Neurosci 2015;9:97
21. Maclaren J, Armstrong BS, Barrows RT, et al. Measurement and correction of microscopic head motion during magnetic resonance imaging of the brain. PLoS One 2012;7:e48088
22. White N, Roddey C, Shankaranarayanan A, et al. PROMO: real-time prospective motion correction in MRI using image-based tracking. Magn Reson Med 2010;63:91-105
23. Herbst M, Maclaren J, Lovell-Smith C, et al. Reproduction of motion artifacts for performance analysis of prospective motion correction in MRI. Magn Reson Med 2014;71:182-190
24. Johnson PM, Liu J, Wade T, Tavallaei MA, Drangova M. Retrospective 3D motion correction using spherical navigator echoes. Magn Reson Imaging 2016;34:1274-1282
25. Kochunov P, Lancaster JL, Glahn DC, et al. Retrospective motion correction protocol for high-resolution anatomical MRI. Hum Brain Mapp 2006;27:957-962
26. Welch EB, Manduca A, Grimm RC, Ward HA, Jack CR Jr. Spherical navigator echoes for full 3D rigid body motion measurement in MRI. Magn Reson Med 2002;47:32-41

27. Haskell MW, Cauley SF, Wald LL. TArgeted Motion Estimation and Reduction (TAMER): data consistency based motion mitigation for MRI using a reduced model joint optimization. IEEE Trans Med Imaging 2018;37:1253-1265
28. Lee D, Lee J, Ko J, Yoon J, Ryu K, Nam Y. Deep learning in MR image processing. Investig Magn Reson Imaging 2019;23:81-99
29. Wang C, Liang Y, Wu Y, Zhao S, Du YP. Correction of out-of-FOV motion artifacts using convolutional neural network. Magn Reson Imaging 2020;71:93-102
30. Pawar K, Chen Z, Shah NJ, Egan GF. Motion correction in MRI using deep convolutional neural network. ISMRM Scientific Meeting & Exhibition, 2018:1174
31. Pawar K, Chen Z, Shah NJ, Egan GF. MoCoNet: motion correction in 3D MPRAGE images using a convolutional neural network approach. arXiv preprint arXiv:1807.10831, 2018
32. Pawar K, Chen Z, Shah NJ, Egan GF. Suppressing motion artefacts in MRI using an Inception-ResNet network with motion simulation augmentation. NMR Biomed 2019:e4225
33. Sommer K, Brosch T, Wiemker R, et al. Correction of motion artifacts using a multi-resolution fully convolutional neural network. ISMRM Scientific Meeting & Exhibition, 2018:1175
34. Duffy BA, Zhao L, Toga A, Kim H. Deep learning based motion artifact correction improves the quality of cortical reconstructions. ISMRM Scientific Meeting & Exhibition, 2019:4426
35. Tamada D, Kromrey ML, Ichikawa S, Onishi H, Motosugi U. Motion artifact reduction using a convolutional neural network for dynamic contrast enhanced MR imaging of the liver. Magn Reson Med Sci 2020;19:64-76
36. Haskell MW, Cauley SF, Bilgic B, et al. Network accelerated motion estimation and reduction (NAMER): convolutional neural network guided retrospective motion correction using a separable motion model. Magn Reson Med 2019;82:1452-1461
37. Godenschweger F, Kagebein U, Stucht D, et al. Motion correction in MRI of the brain. Phys Med Biol 2016;61:R32-56
38. Hedley M, Yan H. Motion artifact suppression: a review of post-processing techniques. Magn Reson Imaging 1992;10:627-635
39. Hashemi RH. Bradley WGJ, Lisanti CJ. MRI: the basics. 2nd ed. Philadelphia: Lippincott Williams & Wilkins, 2004:201-202
40. Armanious K, Jiang C, Fischer M, et al. MedGAN: medical image translation using GANs. Comput Med Imaging Graph 2020;79:101684
41. Kustner T, Armanious K, Yang J, Yang B, Schick F, Gatidis S. Retrospective correction of motion-affected MR images using deep learning frameworks. Magn Reson Med 2019;82:1527-1540
42. Ronneberger O, Fischer P, Brox T. U-net: convolutional networks for biomedical image segmentation. International Conference on Medical Image Computing and Computer-Assisted Invervention, 2015:234-241
43. Lee H, Ryu K, Nam Y, Lee J, Kim DH. Reduction of respiratory motion artifact in C-spine imaging using deep learning: is substitution of navigator possible? ISMRM Scientific Meeting & Exhibition, 2018:2660
44. Kromrey ML, Tamada D, Johno H, et al. Reduction of respiratory motion artifacts in gadoxetate-enhanced MR with a deep learning-based filter using convolutional neural network. Eur Radiol 2020;30:5923-5932
45. Johnson PM, Drangova M. Motion correction in MRI using deep learning. ISMRM Scientific Meeting & Exhibition, 2018:4098
46. Duffy BA, Zhang W, Tang H, et al. Retrospective correction of motion artifact affected structural MRI images using deep learning of simulated motion. 1st Conference on Medical Imaging with Deep Learning (MIDL), 2018
47. Armanious K, Jiang C, Fischer M, et al. MedGAN: medical image translation using GANs. arXiv preprint arXiv:1806.06397, 2018
48. Usman M, Latif S, Asim M, Lee BD, Qadir J. Retrospective motion correction in multishot MRI using Generative Adversarial Network. Sci Rep 2020;10:4786
49. Dou Q, Feng X, Wang Z, Weller D, Meyer C. Deep learning motion compensation for Cartesian and spiral trajectories. ISMRM Scientific Meeting & Exhibition, 2019
50. Bydder M, Ghodrati VK, Ali FA, Hu P. Deep CNN for outlier detection: a complementary tool to low-rank based methods for reducing motion artefacts. ISMRM Scientific Meeting & Exhibition, 2019:0934
51. Vahedipour K, Shah NJ, Stöcker T. Fast MR simulations with JEMRIS 2.1 - disclosing the secrets of MRI sequence development. ISMRM Scientific Meeting & Exhibition, 2009:3039
52. Liu F, Kijowski R, Block WF. MRiLab: performing fast 3D parallel MRI numerical simulation on a simple PC. ISMRM Scientific Meeting & Exhibition, 2013:2072
53. Rodriguez-Molinero A, Narvaiza L, Ruiz J, Galvez-Barron C. Normal respiratory rate and peripheral blood oxygen saturation in the elderly population. J Am Geriatr Soc 2013;61:2238-2240